Experiment and Prediction: A Productive Symbiosis in Studies on the Thermodynamics of DNA Oligomers[†]

Ernesto Carrillo-Nava,[‡,§] Ludger Busch,[‡] Yamilet Mejía-Radillo,[‡,§] Kristian Boehm,[‡,§] and Hans-Jürgen Hinz*[,‡,§]

Institut für Physikalische Chemie der Westfälischen Wilhelms-Universität Münster, Corrensstrasse 30, 48149 Münster, Germany, and Center for Nanotechnology (CeNTech), Heisenbergstrasse 11, 48149 Münster, Germany

Received: January 15, 2010; Revised Manuscript Received: August 17, 2010

Recently, we reported the kinetics of hybridization of cDNA dodecamers (Carrillo-Nava, E.; Mejía-Radillo, Y.; Hinz, H.-J. *Biochemistry* **2008**, *47*, 13153−13157). In this study, we provide the thermodynamic reaction parameters of those dodecamers as well as a comparison with parameters for 24-mers designed from two identical dodecamers in tandem arrangement. The thermodynamic properties were determined by isothermal titration calorimetry (ITC), differential scanning microcalorimetry (DSC), and UV melting studies. On the basis of the results from our kinetic studies, fitting algorithms of DSC and UV melting profiles employed the two-state assumption for the duplex to a single strand dissociation reaction. The formation of both 12-mer and 24-mer duplexes is strongly enthalpy driven at all temperatures. At identical temperatures, the hybridization enthalpy of the 24-mer is within error limits twice that of the 12-mer. Duplex formation is always associated with a significant negative heat capacity change, ΔC_p, which, on a mass basis, is comparable to that observed for protein folding. Only a small part of the favorable reaction enthalpy appears as a standard Gibbs free energy change due to large compensating negative entropy changes linked to duplex formation. On the basis of the results of the present studies, it appears to be absolutely essential for a proper analysis of thermodynamic parameters of oligonucleotide hybridization reactions to combine low temperature ITC measurements of binding enthalpies with DSC and UV melting studies to obtain an accurate assessment of standard Gibbs energy changes or, equivalently, hybridization constants over a broad temperature range. The experimental thermodynamic parameters were compared with theoretical estimates based on nearest-neighbor approximations employing temperature-independent enthalpies. Good agreement between experimental and predicted $\Delta G°$ values is observed at ambient temperatures (20−30 °C), as long as helix formation is associated with small molar heat capacity changes. If the experimental ΔC_p values determined by ITC are taken into account, significant deviations occur.

Introduction

Characterization of the thermodynamics of DNA oligonucleotide duplex formation has been a major effort of DNA research for decades. Early studies focused mainly on the understanding of the nature of the intra- and intermolecular forces determining the structures and structural changes of single- and multiple-stranded ensembles as well as on the mechanisms underlying the processing of genetic information.[2−11] Today, there is renewed practical interest in the topic due to the specificity and programmability of DNA interactions features that are fundamental to optimizing modern DNA-based technology such as polymerase chain reaction (PCR), rolling circle amplification (RCA), in situ hybridization, and chip- and nanoparticle-based applications in science and medicine.[12−22] A particular significance of quantitative information on thermodynamic parameters also stems from the usage of these data as the basis for nearest-neighbor schemes predicting DNA duplex stability, as modern experimental biotechnology relies strongly upon the enormous selectivity that can be achieved in hybridization events.[23−28] There is, however, a caveat that needs to be taken seriously. The quality of the thermodynamic predictions from sequence data depends critically on the accuracy of the thermodynamic parameters used as input data. Until now, most of the data employed in the prediction schemes have been derived indirectly from temperature-dependent properties of melting processes by assuming a model for the reaction mechanism, in most cases the two-state model. While this is likely to apply to dissociation of short duplexes, its application to longer oligomeric duplexes must be verified in each case.

Another particularly critical parameter that has been neglected frequently is the temperature dependence of the enthalpy change, ΔC_p. Its disregard has various reasons. For example, practically all algorithms for the analysis of UV melting curves assume temperature-independent enthalpies, because the resolution of these curves almost never allows an unambiguous discrimination between temperature-dependent and temperature-independent values.[29−39] In the past, there were also experimental constraints. Older differential scanning calorimetry (DSC) studies could not resolve heat capacity changes of DNA duplex dissociation reactions due to instrumental limitations. This situation has changed with modern DSC equipment as well as with the usage of highly sensitive isothermal titration calorimeters (ITC).[40,41]

[†] Part of the "Robert A. Alberty Festschrift".

* To whom correspondence should be addressed. Tel: + 49 251 719730. Fax: +49 251 5355136. E-mail: hinz@uni-muenster.de.

[‡] Institut für Physikalische Chemie der Westfälischen Wilhelms-Universität Münster.

[§] Center for Nanotechnology (CeNTech).

10.1021/jp100412a © 2010 American Chemical Society
Published on Web 09/14/2010

TABLE 1: Sequence and Physical Parameters of the DNA Single Strands Used in the Present Study

sequence	name	ε_{260} (M^{-1} cm^{-1})	MW (g mol^{-1})
5′-**TAG G**TC AAT ACT-3′	**Ia**	120600	3644
3′-**ATC C**AG TTA TGA-5′	**Ib**	123200	3644
5′-**ATC C**TC AAT ACT-3′	**IIa**	114300	3724
3′-**TAG G**AG TTA TGA-5′	**IIb**	128500	3564
5′-TAG GTC AAT ACT TAG GTC AAT ACT-3′	**IIIa**	240600	7351
3′-ATC CAG TTA TGA ATC CAG TTA TGA-5′	**IIIb**	243000	7351

As principally there is no disagreement about the significance of ΔC_p values for the correct prediction of transition enthalpies, transition entropies, and, consequently, standard Gibbs energy changes, that is, equilibrium constants, at a specific temperature, it has been repeatedly emphasized that particular care should be taken for their correct determination.[42−46]

In the present study, we complement our previous stopped-flow measurements of the on-rate constants and activation energies of 12-mer hybridization with the thermodynamic parameters describing the equilibrium situation.[1] We placed particular emphasis on quantifying the heat capacity change associated with the duplex formation of DNA oligomers. Furthermore, we addressed the question of additivity of thermodynamic parameters derived from short oligomers to predict stabilities of longer duplexes. For that purpose, we constructed a DNA oligomer that consists of two identical 12-mers in tandem arrangement. This 24-mer cannot self-associate nor can it form hairpins or other intermediate structures, a property that facilitates the interpretation of enthalpy and heat capacity phenomena.

The thermodynamics of self-assembly of the 12-mer and 24-mer DNA duplexes from complementary single strands have been investigated by titration microcalorimetry (ITC) and DSC in conjunction with van't Hoff analysis of UV temperature scans of double and single strands. While the UV melting studies could not resolve heat capacity changes as expected, the ITC and DSC measurements revealed significant negative ΔC_p values for duplex formation, which, in our case, cannot be accounted for by intrinsic structural changes of the single strands.

Materials and Methods

Oligonucleotide Preparation and Characterization. The sequences of the oligonucleotides studied together with their molar absorption coefficients at 260 nm, ε_{260}, and their molar masses are shown in Table 1. The 12-mers differ by the position of the four bases marked in bold. They occur at either the 3′ or the 5′ end. The residual eight bases are identical. The single strands were designed in such a manner that none of them can form hairpins or can hybridize with the complementary strand out of register.

The oligonucleotides were synthesized using standard phosphoramidite chemistry.[47] The syntheses were carried out in an ABI-392-08-DNA synthesizer (Applied Biosystems, Weiterstadt, Germany) on a 1 μmol scale following the synthesis protocol for 3′-cyanoethyl phosphoramidites. The coupling efficiency was always higher than 99%. They were purified using a LiChroCART 250-4 column with a Merck-Hitachi HPLC pump model 655A-12 connected with a variable wavelength monitor (model 655-A) and a controller (model D-2000). The oligonucleotides were purified in a triethylamine acetate buffer with an acetonitrile gradient and lyophilized in a centrifuge under vacuum. The purity and composition of each oligonucleotide were verified by mass spectrometry using matrix-assisted laser desorption ionization (MALDI). The purity of the oligonucleotides was 99.98%. DNA concentrations were determined spectrophotometrically by measuring the absorbance at 260 nm and using the corresponding extinction coefficients given in Table 1. They were calculated on the basis of the nearest-neighbor approximation.[48,49]

Equal amounts of the complementary single strands were mixed in buffer to obtain solutions of known concentrations of the oligonucleotide duplexes. Three buffer systems were employed to identify (a) the effect of Mg^{2+} ions and (b) a possible intrinsic effect on the thermodynamic parameters of different buffering agents. The buffer systems were a standard phosphate buffer (10 mM NaH_2PO_4 and 100 mM NaCl, pH 7.0) and two cacodylate buffers, one with $MgCl_2$ [10 mM $MgCl_2$, 10 mM $(CH_3)_2AsONa$, and 100 mM NaCl, pH 7.0] and the other without $MgCl_2$ [10 mM $(CH_3)_2AsONa$ and 100 mM NaCl, pH 7.0].

ITC. The binding reactions were conducted using a VP-ITC from MicroCal (Northampton, MA). Prior to experiments, all solutions (titrant and titrand) were degassed for 15 min while stirring under vacuum. Titrations were carried out by injecting 10 μL portions of the complementary oligonucleotide into the single strand solution in the calorimetric cell. Single strand concentrations in the cell were of the order of 3 μM, and the concentrations of the solutions in the syringe were at least six times higher. The equilibration period after each injection was 420 s. This time had been determined as sufficiently long for the reaction to proceed to completion in preliminary experiments. Integration of the differential power signals with respect to time yields the apparent heat changes per injection. Generally, the titrations were continued beyond the point of saturation to obtain values for the heat of dilution of the titrant. The averaged heat of dilution value was subtracted from each heat peak before the titration data were further processed to obtain molar enthalpy values and titration curves using Origin version 7.0 and the ITC Data Analysis software in Origin macros version 5.0.[50−52]

Because of the complementarities of the DNA single strands, we could use the "one class of identical sites model" for the analysis of the titration data.[51] The corrected heat evolved per injection, Q (the experimental heat minus the heat of dilution), is fitted to the equation below

$$Q = \frac{nC_t\Delta H^\circ V_o}{2}\left\{1 + \frac{X_t}{nC_t} + \frac{1}{KnC_t} - \left[\left(1 + \frac{X_t}{nC_t} + \frac{1}{KnC_t}\right)^2 - \frac{4X_t}{nC_t}\right]^{1/2}\right\} \quad (1)$$

where K is the binding constant, n characterizes the stoichiometry of the hybridization reaction, V_o is the active cell volume, C_t is the total single strand concentration of the oligonucleotides in the reaction cell, ΔH° is the standard molar enthalpy change of hybridization, and X_t is the strand concentration of the complementary oligonucleotide in the syringe. For oligonucleotides of equal length, the stoichiometry should be $n = 1$. However, in the fitting routine, n was allowed to vary in order to verify independently the active oligonucleotide concentration. A nonlinear regression fit of the experimental data to eq 1 yields n, K, and ΔH°. Standard Gibbs energy changes and entropy changes were calculated at temperature T using the relations

$$\Delta G^\circ = -RT \ln K \tag{2}$$

and

$$\Delta S^\circ = \frac{\Delta H^\circ - \Delta G^\circ}{T} \tag{3}$$

The various ITC hybridization experiments were carried out in phosphate buffer with closely similar final duplex concentrations to minimize variations in the degree of complex formation.

DSC. The scanning calorimetric experiments were performed using a CSC 6100 Nano II DSC (Provo, UT). Prior to the scans, all solutions were degassed while they were stirred under vacuum. An excess pressure of 3 atm was applied to the cells during scanning. DSC scans were performed from 10 to 85 °C at a scan rate of 1 K min^{-1}. The double helix concentration was 50 μM. Buffer versus buffer scans were performed prior to the DNA scans. Sample scans were routinely executed two or three times to check for repeatability. The heat capacity profiles were analyzed after subtraction of the buffer versus buffer scans. The pre- and post-transition baselines were established from independent linear least-squares fits to the data points of the pre- and post-transition regions. Then, the sigmoidal baseline under the transition peak was constructed taking into account the profile of the transition peak and the experimental pre- and post-transition baselines. The calorimetric enthalpy, ΔH_{cal}, was determined by integration of the area between the peak and the sigmoidal baseline; T_m refers to the temperature where 50% of the transition has occurred.[53] The heat capacity difference, ΔC_p, between double and single strands was determined from the difference between the pre- and the post-transitional baselines at T_m. All calorimetric melting profiles were analyzed using the software supplied with the instrument (CpCalc version 2.1, Applied Thermodynamics) for the "AB = A + B" model.

The apparent heat capacity difference, $\Delta C_{p,\,app}$, is given by eq 4

$$\Delta C_{p,app} = c_{p,buffer} m_{buffer} - c_{p,oligonucleotide} m_{oligonucleotide} \tag{4}$$

where m_{buffer} and $m_{oligonucleotide}$ are, respectively, the mass of the replaced buffer and the oligonucleotide, and $c_{p,\,buffer}$ and $c_{p,\,oligonucleotide}$ are the specific heat capacities of the buffer and the oligonucleotide.[53] Introducing the specific volume and solving for the heat capacity of the oligonucleotide, one obtains the equation

$$c_{p,oligonucleotide} = c_{p,buffer}\left(\frac{v_{oligonucleotide}}{v_{buffer}}\right) - \frac{\Delta C_{p,app}}{m_{oligonucleotide}} \tag{5}$$

At low buffer concentration, the heat capacity of the buffer is not very different from the heat capacity of water. As long as no absolute values of heat capacity are required but only transition parameters such as enthalpies or entropies, approximate average values for the specific volumes may be employed. For our data analysis, we used a value of 0.54 cm^3 g^{-1} for the oligonucleotides and 1 cm^3 g^{-1} for the buffer.[54]

The calorimetric melting profiles of the double strands were fitted to a two state transition model DS $\rightleftarrows$ 2SS, where DS represents the duplex state and SS refers to the single strand state. The algorithm is incorporated in the CpCalc program that is provided with the Nano-DSC. The van't Hoff enthalpy, ΔH_{vH}, was determined by fitting the experimental calorimetric profile to the following expression

$$c_p = \frac{dF_{SS}}{dT}\Delta H_{vH} \tag{6}$$

where F_{SS} is the fraction of molecules in the single-stranded state. The value of F_{SS} at different temperatures can be written in terms of the experimentally known total duplex concentration of DNA, C_T, and calculated numerically with the expression

$$\frac{F_{SS}}{(1 - F_{SS})^{1/n}} = \frac{K^{1/n} C_T^{(1/n)-1}}{n^{1/n}} \tag{7}$$

In a DSC experiment, one directly obtains a heat capacity (C_p) vs temperature curve that can be converted into a (C_p/T) vs T curve. Integration of the excess heat capacity peak provides the transition enthalpy ΔH_{T_m}, integration of the converted curve the transition entropy. The heat capacity difference at the melting temperature between the extrapolated linear baselines of pure duplexes and the pure single strands yields ΔC_p. Using these data, the standard Gibbs energy change, ΔG°, can be calculated at any temperature employing the relationship

$$\Delta G^\circ(T) = \Delta G_{T_m}{}^\circ + \Delta H^\circ_{T_m}\left(1 - \frac{T}{T_m}\right) + \int_{T_m}^{T} \Delta C_p \, dT - T\int_{T_m}^{T} \Delta C_p \, d \ln T \tag{8}$$

UV Melting Curves. Melting experiments were performed following the absorption at 260 nm in a X-Dap 1024 diode array spectrophotometer (Axeon GmbH, Bottrop, formerly IKS-Optoelektronik). Typically, the samples were heated from 5 to 75 or 85 °C at a rate of 0.5 or 1.0 K min^{-1} with identical results for the different heating rates. Different optical path lengths (from 0.1 to 10 mm) were used due to the broad range of DNA concentrations studied. To avoid condensation of moisture at temperatures below 20 °C, a constant flow of dry nitrogen was provided to the chamber where the optical cells were located.

Thermodynamic analysis was based on the two-state model, as in the case of the DSC experiments. The experimentally observed absorbance, A_{obs}, was fitted to the following equation

$$A_{obs} = x_{SS} A_{SS} + (1 - x_{SS}) A_{DS} \tag{9}$$

where x_{SS} is the mole fraction of single-stranded oligonucleotides, A_{SS} is the average absorbance of the single strands, and A_{DS} is the absorbance of the duplex. The temperature dependence of the fraction of single strands can be obtained from expressions 10 and 11:

$$x_{SS} = \left(\frac{2K}{C_T} + \frac{K^2}{C_T{}^2}\right)^{1/2} - \frac{K}{C_T} \tag{10}$$

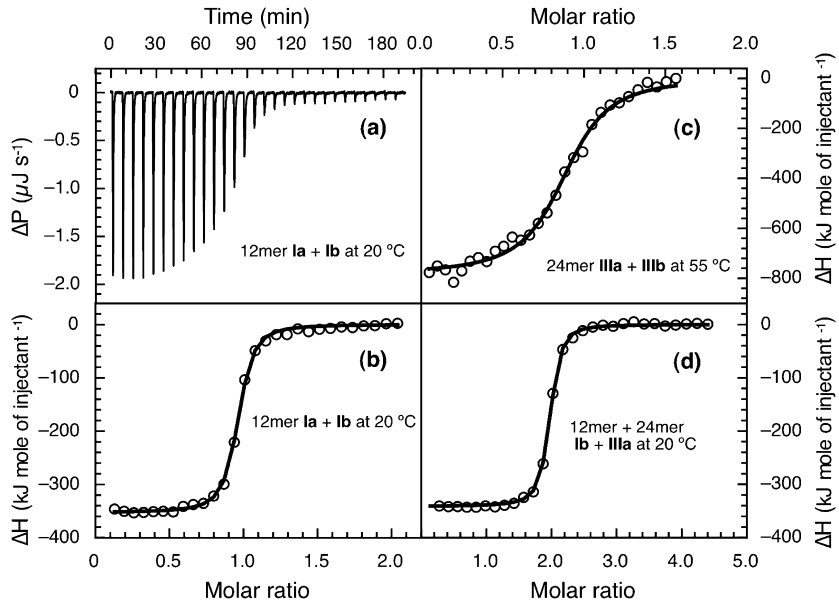

Figure 1. Representative ITC measurements on duplex formation between complementary 12-mers and 24-mers. (a) Titration of strand **Ia** (2 μM) with **Ib** (18 μM) in a 100 mM NaH_2PO_4 and 100 mM NaCl, pH 7.0, buffer at 20 °C. (b) The integrated and normalized data (open circles) and the resulting binding isotherm (solid line) of the 12-mer depicted under panel a. (c) Integrated and normalized data (open circles) of the single strand **IIIa** (2 μM) titrated with the complementary strand **IIIb** (15 μM) in 100 mM NaH_2PO_4 and 100 mM NaCl, pH 7.0, buffer at 55 °C. (d) 24-mer strand **IIIa** (2.5 μM) titrated with the complementary 12-mer strand **Ib** (45 μM) in 100 mM NaH_2PO_4 and 100 mM NaCl, pH 7.0, buffer at 20 °C.

$$\frac{\mathrm{d}\ln K}{\mathrm{d}T} = \frac{\Delta H_{\mathrm{vH}}}{RT^2} \tag{11}$$

K is the equilibrium constant for the two-state hybridization reaction and C_T is the total concentration of oligonucleotide strands. The van't Hoff expression provides the link between the van't Hoff enthalpies and the fraction of single strands, x_{SS}.

Integration of eq 11, employing a linearly temperature-dependent $\Delta H°$, yields eq 12. Together with eqs 9 and 10, it was used for the analysis of the melting curves.

$$K = \left(\frac{4}{C_T}\right)\exp\left\{-\frac{\Delta H^\circ}{RT}\left(1 - \frac{T}{T_m}\right) + \frac{\Delta C_p}{RT}\left[T_m - T + T\ln\left(\frac{T}{T_m}\right)\right]\right\} \tag{12}$$

The melting curve analysis was not sensitive to even significant variations of ΔC_p. Therefore, the thermodynamic parameters derived from the UV melting curves listed in Table 4 are temperature-independent values.

Alternatively, we derived thermodynamic parameters from the concentration dependence of the melting temperature, T_m, using the expression

$$\frac{1}{T_m} = \frac{R}{\Delta H^\circ}\ln\left(\frac{4}{C_T}\right) + \frac{\Delta S^\circ}{\Delta H^\circ} \tag{13}$$

where $R = 8.314$ J mol^{-1} K^{-1} is the gas constant, C_T is the total strand concentration, $\Delta H°$ and $\Delta S°$ are the temperature-invariant standard transition enthalpies and entropies, respectively. A plot of $1/T_m$ vs ln $(4/C_T)$ provides $\Delta H°$ from the slope and $\Delta S°$ from the intersection.

Results

ITC. ITC is optimally suited for determining all relevant thermodynamic parameters of duplex formation of DNA oligomers, that is, binding constants, stoichiometry, reaction enthalpies, and heat capacity changes.[50,52] A typical ITC titration is shown in Figure 1a along with the binding isotherm obtained for complex formation at 20 °C between the 12-mers **Ia** and **Ib** (Figure 1b). The analogous binding isotherm for hybridization of the 24-mer single strands **IIIa** and **IIIb** at 55 °C is given in Figure 1c. Figure 1d illustrates complex formation between the 24-mer **IIIa** and the 12-mer **Ib** at 20 °C. We performed ITC measurements in the temperature range between 10 and 25 °C for the 12-mers and between 10 and 55 °C for the 24-mers with the results illustrated in Figure 2. It is evident that for temperatures well below the melting temperatures of the oligonucleotide duplexes the enthalpies of hybridization of both the 24-mer and the 12-mer change linearly with temperature. The temperature coefficients, ΔC_p, are both negative rendering the $\Delta H°$ values more exothermic as the temperature is increased. However, at temperatures above about 20 °C for the 12-mer and above 40 °C for the 24-mer, one observes a deviation from linearity, which results from incomplete duplex formation due to partial melting at these temperatures. Therefore, we determined the ΔC_p values from the linear parts of the $\Delta H°$ vs temperature plots (Figure 2).

As the 24-mer used in the present studies consists of two identical 12-mers linked in tandem manner, we also performed hybridization experiments at 20 and 25 °C in which the 24-mer **IIIa** was titrated with the complementary 12-mer **Ib**. At 20 °C, no melting effects occur. Therefore, the observed $\Delta H°$ values reflect the total hybridization enthalpy of a duplex of 12-mers. The comparison between the enthalpy values in Tables 2 and 3 shows this clearly. The average $\Delta H°$ values observed at 20 °C for titrations of the 24-mer with the 12-mer are within error limits identical to those obtained for the hybridization of the complementary 12-mers at 20 °C. At 25 °C, however, the enthalpy of duplex formation between the 24-mer and the 12-

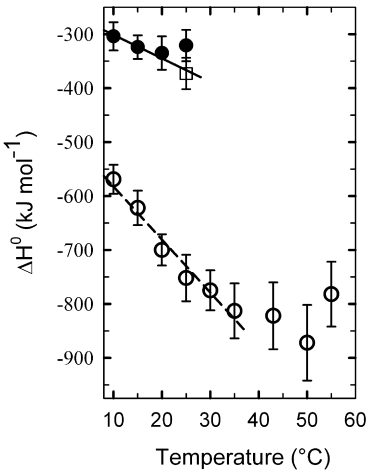

Figure 2. Variation with temperature of the hybridization enthalpies of 12-mers and 24-mers determined by ITC measurements: **Ia** + **Ib** (solid circles); **IIIa** + **IIIb** (open circles); the buffer was 100 mM NaH_2PO_4 and 100 mM NaCl, pH 7.0. The straight and dashed lines illustrate the temperature-independent ΔC_p values. ΔC_p (**Ia** + **Ib**) = −4.4 kJ (mol of dodecamer)$^{-1}$ K^{-1}, and ΔC_p (**IIIa** + **IIIb**) = −9.7 kJ (mol of 24-mer)$^{-1}$ K^{-1}. The open square refers to the enthalpy value at 25 °C obtained by titration of the 24-mer **IIIa** with the 12-mer **Ib**.

TABLE 2: Thermodynamic Parameters for the Hybridization of the Dodecamers Ia and Ib and the 24-mer IIIa and the 12-mer Ib in a 10 mM NaH_2PO_4 and 100 mM NaCl, pH 7.0, Buffer, Measured by ITC

T (°C)	$\Delta H°$ (kJ mol^{-1})	$\Delta S°$ (kJ mol^{-1} K^{-1})	$K_B \times 10^{-8}$ (M^{-1})	$\Delta G°$ (kJ mol^{-1})
12-mer **Ia** titrated with 12-mer **Ib**				
10	−304 ± 26	−0.911	3.19 ± 0.4	−46.1 ± 0.3
15	−324 ± 22	−1.284	2.82 ± 0.2	−45.9 ± 0.2
20	−335 ± 31	−0.982	2.25 ± 0.1	−46.9 ± 0.2
25	−321 ± 29	−0.923	1.10 ± 0.1	−45.9 ± 0.2
24-mer **IIIa** titrated with 12-mer **Ib**				
20	−337 ± 36	−0.996	1.46 ± 0.1	−45.8 ± 0.2
25	−373 ± 29	−1.101	1.04 ± 0.1	−45.8 ± 0.2

mer listed in Table 2 is more negative than the value given for the hybridization of the complementary dodecamers. The observed $\Delta H°$ value for the reaction between the 24-mer and the 12-mer at 25 °C (see open square in Figure 2) rather equals the value that is obtained by linear extrapolation of the low temperature $\Delta H°$ values to 25 °C. The difference between the two enthalpy values at 25 °C is easy to rationalize, as each 24-mer provides two independent 12-mer binding sites. Therefore, the experimental 12-mer concentration is 5.0 μM, two times that of the 24-mer (2.5 μM) and thus more than twice as high as the concentrations that were used in the dodecamer titrations shown in Figure 1b. As a consequence, there is no longer incomplete hybridization at 25 °C, because the melting temperature has increased as a result of the higher binding site concentration.

It is evident that two 12-mers bind to the 24-mer, as the stoichiometry of 2:1 in Figure 1d demonstrates. The enthalpy per mole of 12-mer bound at 20 °C is close to the value observed for hybridization of the complementary 12-mer single strands, supporting the concept of independent binding sites on the 24-mer.

The possibility to determine by ITC in a straightforward manner in addition to enthalpies also binding constants is one of the very useful features of the method.[55,56] However, care has to be taken that the binding constants do not exceed significantly the detection limit of about 10^9 M^{-1} in the direct titration. If they do, the ITC titration curves still look reasonable, but the binding constants obtained from their analysis can be completely off by orders of magnitude. This was observed for the low temperature ITC measurements on the 24-mers. Their analysis provided binding constants that were only larger by a factor of 4 than those obtained for 12-mer hybridization, whereas the correct binding constants for 24-mers are of the order of 10^{18} M^{-1} or higher.

In our experiments, only the binding isotherms obtained at 50 and 55 °C could be evaluated with regard to the hybridization constant of complementary 24-mers. The corresponding values were 0.35×10^8 and 0.23×10^8 M^{-1}, respectively. They provide accurate numerical values of the binding constants at these temperatures.

The thermodynamic parameters obtained in the present ITC studies are summarized in Tables 2 and 3. Several features are worth emphasizing: The exothermic hybridization enthalpies become more negative with increasing temperature for both the 12-mer and the 24-mer system. The corresponding ΔC_p values are −4.4 kJ (mol of 12-mer)$^{-1}$ K^{-1} and −9.7 kJ (mol of 24-mer)$^{-1}$ K^{-1}, respectively, if the temperature invariance of ΔC_p is implied and only the enthalpy values obtained well below the melting temperature are used for its calculation.

At identical temperatures, the enthalpies of duplex formation of the 24-mers are within error limits twice as large as those obtained for the 12-mers. This is to be expected as long as cooperative effects are absent, because the 24-mer is a tandem construction of two 12-mers.

The binding constants observed for the formation of the 12-mer duplexes decrease with increasing temperature as expected from the principle of Le Chatelier for exothermic reactions in that an increase of temperature favors the formation of single strands. Variation of the binding constant with temperature is influenced significantly by the magnitude of ΔC_p. The hybridization constant obtained from the titration of the 24-mer strand **IIIa** with two complementary 12-mers of type **Ib** is rather close to that derived from the titration of two complementary 12-mers of type **Ia** and **Ib**.

DSC. The optimal method for determining enthalpy and heat capacity changes at the melting temperature of DNA duplexes is by DSC measurements.[53] For a quantitative molecular interpretation of the thermodynamic parameters, four measurements are required as follows: (a) the heat capacity measurement of both cells filled with buffer, (b) two temperature scans with the sample cell filled with each single strand, and (c) a DSC scan of the duplex.

A typical heat capacity profile of the helix to coil transition of the dodecamer duplex (**Ia** + **Ib**) is shown in Figure 3a. We observed reversibility of the reaction for all systems studied. Thus, evidently no degradation of the oligonucleotides occurred at the high temperatures that were reached during the scans (up to 80 °C). The calorimetric enthalpy obtained from integration of the transition peak is 351 kJ mol^{-1} at T_m = 49.7 °C, and the heat capacity change is 2.3 kJ mol^{-1} K^{-1}. The deconvolution of the heat capacity peak is illustrated in Figure 3b. We employed the dissociation model without a heat capacity change and obtained a van't Hoff enthalpy of 312 kJ mol^{-1}. The agreement is not perfect but in line with results reported previously for differences between direct calorimetric enthalpies and van't Hoff enthalpies derived from curve fitting to a model. Figure 3c shows apparent heat capacity profiles of the 24-mer single strands. We report here the profiles of the 24-mers, because the possible existence of secondary structure in the

TABLE 3: Thermodynamic Parameters for the Hybridization of the 24-mers IIIa + IIIb in the 10 mM NaH_2PO_4 and 100 mM NaCl, pH 7.0, Buffer, Measured by ITC[a]

T (°C)	10	15	20	25	30	35	43	50	55
$-\Delta H°$ (kJ mol^{-1})	569 ± 27	622 ± 32	700 ± 29	752 ± 43	775 ± 37	813 ± 51	822 ± 62	872 ± 70	782 ± 60

[a] The heat capacity change $\Delta C_p = -9.7$ kJ mol^{-1} K^{-1} is obtained from the enthalpies in the temperature range 10−35 °C. The hybridization constant at 55 °C is 2.3×10^7 M^{-1}, corresponding to $\Delta G° = -46.25$ kJ mol^{-1}.

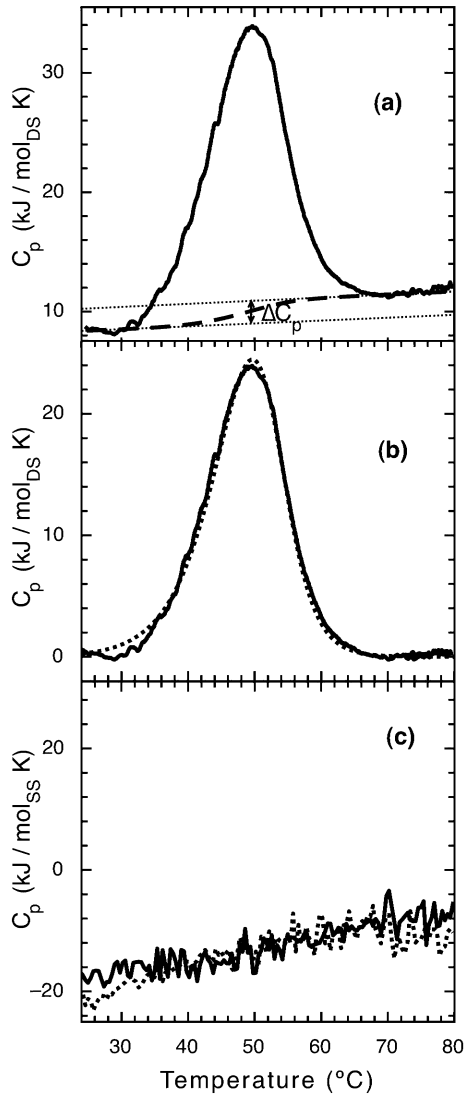

Figure 3. (a) Experimental calorimetric profile (continuous line) of a **Ia** + **Ib** duplex solution (50 μM) in a 100 mM NaH_2PO_4 and 100 mM NaCl, pH 7.0, buffer; heating rate of 1 K min^{-1}. The calorimetric enthalpy obtained by integration of the peak area is $\Delta H_{cal} = 351$ kJ mol^{-1}. The experimental heat capacity change at $T_m = 47.9$ °C is $\Delta C_p = 2.32$ kJ mol^{-1} K^{-1}. Also shown are the baseline for the pre- and post-transitional states (dotted lines), the resulting baseline (broken line), and the ΔC_p at the melting temperature. (b) Deconvolution analysis of the excess heat capacity (dotted lines) of the same system calorimetric profile (continuous line), which has been normalized by subtraction of the baseline. The transition enthalpy at $T_m = 49.01$ °C is $\Delta H_{vH} = 312$ kJ mol^{-1}. (c) Heat capacity scans of 24-mer single strands: **IIIa** (solid line) and **IIIb** (dashed line).

single strands is likely to be more pronounced in 24-mers than in 12-mers. The experimental heat capacity profiles of the single-stranded 24-mers are rather telling. Obviously, heat capacity of the single strands increases gradually at lower temperatures and appears to flatten out at about 80 °C. However, there is no indication of a heat capacity peak that would indicate a transition of the single strands within the experimental temperature range.

A series of DSC studies on duplexes were performed in different buffers with the results summarized in Table 4. We reported in our previous study on the kinetics of hybridization an influence of the buffer system on the on-rate constant and activation parameters of strand association.[1] A similar influence is also observed with regard to the thermodynamic equilibrium parameters, in that the enthalpies are tendentiously smaller in cacodylate buffer than in phosphate buffer. In particular, the presence of Mg^{2+} ions does not only increase the transition temperature, it also increases the transition enthalpy significantly. It is important to note that we observed positive heat capacity changes for helix melting in all buffers. The magnitude of ΔC_p equals 2.3 kJ mol^{-1} K^{-1} for the 12-mers at T_m in phosphate buffer A. This ΔC_p value is smaller than that observed by ITC at lower temperatures. Similar differences were reported previously by Holbrook et al.[57]

UV Melting Experiments. As the majority of thermodynamic parameters on oligonucleotide DNA helix−coil transitions in the literature was derived from UV melting studies, we also performed such measurements to check for intrinsic differences between the various methods.

Figure 4a shows the normalized melting curves of the 12-mer and 24-mer duplexes, and Figure 4b provides the corresponding UV temperature scans of the single strands. Whereas the melting curves of the duplexes exhibit the typical sigmoidal shape of cooperative transitions, the UV absorption of the single strands increases gradually with temperature without any indication of even an uncooperative melting transition in the relevant temperature range. This finding parallels that observed by DSC, where the heat capacity profiles of the single strands also failed to show any indication of a transition.

Figure 5 presents the $1/T_m$ vs ln $(4/C_T)$ plots of the duplexes in various buffer systems. Thermodynamic parameters derived from these plots are included in Table 4.

The following general conclusions can be drawn from the UV melting curves. For all of the systems studied, there was a pronounced dependence on the concentration of the melting temperature. The melting temperature increased with the increase of the total concentration of oligonucleotides as expected for a bimolecular process.[1] The presence of Mg^{2+} ions increased both the stability of the double helix and the hybridization enthalpy. The stability increase is reflected in higher transition temperatures as well as in higher standard Gibbs energy changes, $\Delta G°$. The slight difference in the primary structure between the sequences **I** and **II** also has a measurable effect on the thermodynamic properties. Particularly, in the presence of Mg^{2+} ions, there are differences between the dodecameric duplexes. This observation is analogous to the findings in our study on the kinetics of hybridization, where the on-rates of duplex formation and their temperature dependence were found to depend significantly on the sequence of the dodecamers.

Inspection of Figure 4 reveals that by doubling the number of base pairs from 12 (sequences **Ia** and **Ib**) to 24 (sequences **IIIa** and **IIIb**) the melting temperature of the double helix is raised notably. However, the shape of the melting curve has not changed visibly; it is still compatible with melting in a single

TABLE 4: Thermodynamic Parameters for the Association of the Duplexes in Different Buffers, Obtained from DSC Measurements[a]

	duplex **Ia** + **Ib**			duplex **IIa** + **IIb**			duplex **IIIa** + **IIIb**		
buffer	T_m (°C)	$-\Delta H_{cal}$ (kJ mol^{-1})	$-\Delta C_p$ (kJ mol^{-1} K^{-1})	T_m (°C)	$-\Delta H_{cal}$ (kJ mol^{-1})	$-\Delta C_p$ (kJ mol^{-1} K^{-1})	T_m (°C)	$-\Delta H_{cal}$ (kJ mol^{-1})	$-\Delta C_p$ (kJ mol^{-1} K^{-1})
A	49.62 ± 0.02 (49.01)[b] (49.8)[c]	351 ± 11 (312)[b] (364)[c] (349)[d]	2.32 ± 0.11	47.90 ± 0.03 (48.12)[b] (45.8)[c]	353 ± 21 (380)[b] (364)[c]	3.80 ± 0.33	65.10 ± 0.4	792 ± 35.3	3.95
B	55.94 ± 0.20 (56.45)[b] (55.9)[c]	402 ± 3.8 (350)[b] (417)[c] (405)[d]	2.0 ± 0.70	53.29 ± 0.02 (53.30)[b] (51.9)[c]	395 ± 28 (374)[b] (400)[c] (439)[d]	2.2 ± 4.52			
C	49.14 ± 0.09 (49.96)[b] (48.7)[c]	335 ± 15.4 (344)[b] (351)[c]M (349)[d]	1.3 ± 0.21	49.14 ± 0.01 49.90[b] (47.7)[c]	331 ± 6.8 (348)[b] (391)[c] (329)[d]	1.8 ± 0.28			

[a] Data from van't Hoff analysis of DSC and UV melting curves are included in brackets. The duplex concentration was 50 μM in all experiments. Buffer A: 10 mM NaH_2PO_4 and 100 mM NaCl, pH 7.0; buffer B: 10 mM $MgCl_2$, 10 mM $(CH_3)_2AsONa$, and 100 mM NaCl, pH 7.0; and buffer C: 10 mM $(CH_3)_2AsONa$ and 100 mM NaCl, pH 7.0. [b] van't Hoff enthalpy (ΔH_{vH}) and melting temperature values obtained from the deconvolution of the heat capacity scans using eq 6. [c] van't Hoff enthalpies and melting temperatures derived from UV melting curves. [d] Temperature invariant $\Delta H°$ determined from variation of T_m with concentration using eq 13.

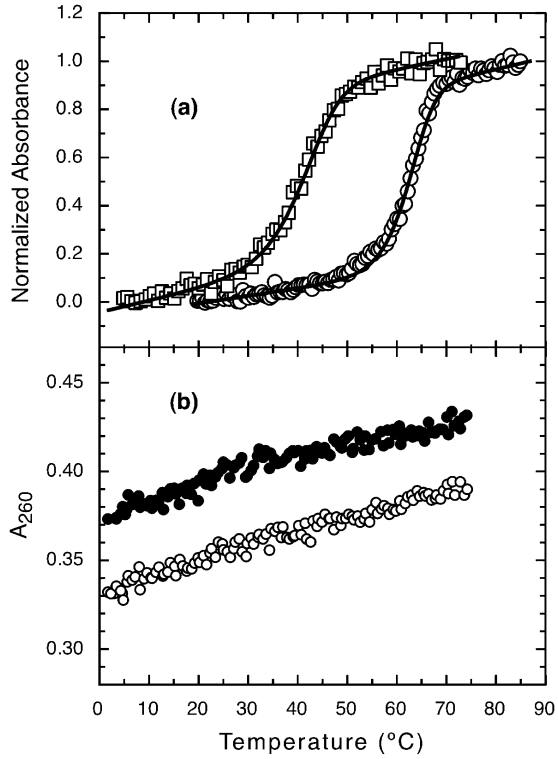

Figure 4. (a) Normalized UV melting scans of 12-mer (**Ia** + **Ib**) duplex (open squares) and of the 24-mer duplex **IIIa** + **IIIb** (open circles). The total single strand concentration of the 12-mers was 3.8 μM, and the duplex concentration was 1.6 μM. The total single strand concentration of the 24-mers was 3.0 μM, and the double strand concentration was 1.5 μM. The full lines represent fits of the data to eq 8. (b) UV melting scans of the 24-mer single strands **IIIa** (solid dots) (1.68 μM) and **IIIb** (open circles) (1.46 μM). All experiments were done in the 10 mM NaH_2PO_4 and 100 mM NaCl, pH 7.0, buffer using a heating rate of 0.5 K min^{-1}.

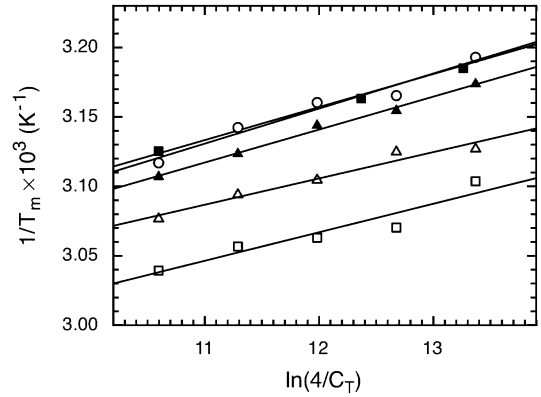

Figure 5. Concentration dependence of the reciprocal melting temperatures of the 12-mer duplexes (**Ia** + **Ib**) and (**IIa** + **IIb**) in different buffers. The black filled squares represent the **IIa** + **IIb** duplex in a 10 mM NaH_2PO_4 and 100 mM NaCl, pH 7.0, buffer; the black filled triangles represent the **Ia** + **Ib** duplex in a 10 mM $(CH_3)_2AsONa$ and 100 mM NaCl, pH 7.0, buffer; the open circles represent the **IIa** + **IIb** duplex in a 10 mM $(CH_3)_2AsONa$ and 100 mM NaCl, pH 7.0, buffer; the open squares represent the **Ia** + **Ib** duplex in a 10 mM $MgCl_2$, 10 mM $(CH_3)_2AsONa$, and 100 mM NaCl, pH 7.0, buffer; and the open triangles represent the **IIa** + **IIb** duplex in a 10 mM $MgCl_2$, 10 mM $(CH_3)_2AsONa$, and 100 mM NaCl, pH 7.0, buffer.

step. The van't Hoff enthalpy values obtained from both the analysis of the heat capacity profile and the UV melting curve of the 24-mer are similar but smaller than the calorimetric enthalpy values obtained from our ITC measurements.

Discussion

Comparison of Hybridization Enthalpies and Heat Capacity Changes. Inspection of the enthalpy data obtained by ITC, DSC, and from the analysis of UV melting curves suggests several conclusions of general importance. The most reliable enthalpy values at low temperature are obtained by ITC measurements, whereas at the melting temperature the direct calorimetric transition enthalpies derived from integration of the excess heat capacity profile are likely to be the best estimates.

As the 24-mer employed in our studies consists of two identical 12-mers in tandem arrangement, one would expect hybridization enthalpies twice as large as those observed for the formation of the corresponding 12-mer duplexes. This expectation is met within the limits of error of the ITC experiments, as a comparison of the enthalpies for 12-mers and 24-mers at the same temperature shows. The enthalpies for both 12-mer and 24-mer duplex formation are strongly temperature dependent with characteristic negative heat capacity changes of -4.4 kJ (mol of 12mer)$^{-1}$ K^{-1} and -9.7 kJ (mol of 24mer)$^{-1}$ K^{-1}, respectively, if temperature invariance is assumed for ΔC_p.

It is informative to compare the ΔC_p values obtained in the present study with data from the literature. As most data reported there were listed for helix disruption, we take the positive values

and we also convert the molar ΔC_p values to numbers that refer to 1 mol of base pairs to facilitate the comparison. The resulting temperature-independent specific heat capacity changes, Δc_p, are as follows: 367 J (mol base pair)$^{-1}$ K^{-1} for a base pair in the 12-mer and 404 J (mol base pair)$^{-1}$ K^{-1} for a base pair in the 24-mer. Literature data show a great variety of Δc_p values. For disruption of base pairs of polymeric hetero- and homoduplexes, Chalikian et al.[43] reported on the basis of DSC studies an average value of 270 J (mol base pair)$^{-1}$ K^{-1} with an error of 90 J (mol base pair)$^{-1}$ K^{-1}. Schöppe et al.[58] observed by DSC heat capacity changes of 490 J (mole of base pair)$^{-1}$ K^{-1} for DNA 12-mers with alternating A and T triplets. For calf thymus DNA, the values were $\Delta c_p = 75$ J (mol base pair)$^{-1}$ K^{-1} at 100 mM NaCl and $\Delta c_p = 120$ J (mol base pair)$^{-1}$ K^{-1} at 1 M NaCl in 10 mM phosphate buffer, pH 7.0. Lang and Schwarz determined heat capacity changes on 10-mers by ITC and found a value of 140 ± 9 J (mol base pair)$^{-1}$ K^{-1}.[44] Recent ITC measurements on the hybridization of 8-mers by Kaur et al.[46] resulted in a Δc_p value of 90 J (mol base pair)$^{-1}$ K^{-1}. Holbrook et al.[57] derived from ITC studies on 14-mers a heat capacity change of 389 J (mol base pair)$^{-1}$ K^{-1} for the temperature range between 9 and 39 °C. DSC measurements on the same 14-mers resulted in a specific heat capacity change at $T_m = 66$ °C of 239 J (mol base pair)$^{-1}$ K^{-1}. In summary, one can state that specific heat capacity changes were reported to lie between zero and about 500 J (mol base pair)$^{-1}$ K^{-1}.

As most current nearest-neighbor schemes for predicting DNA duplex stability have assumed $\Delta c_p = 0$,[23−28] it is obvious that significant errors can be involved in the stability predictions, if heat capacity changes are of the order of a couple of hundred J (mol of base pair)$^{-1}$ K^{-1}. On the basis of our studies[58] and the evidence from the large number of careful investigations cited above, we assume that all duplex disruptions are associated with a heat capacity change. Its magnitude will depend on the sequence as well as on the environmental parameters, such as salt concentration and Mg^{2+} ion content, but it will rarely be zero.

It is somewhat surprising that the size of the heat capacity changes associated with protein unfolding are considered large and important and that a great many studies tackle the molecular interpretation of ΔC_p, whereas much less importance is assigned to these values in DNA research. This neglect is unjustified, because the value of ΔC_p for duplex disruption is of comparable magnitude as the values observed for protein unfolding, if the comparison is conducted on a mass basis. For example, assuming a molar mass of 20000, the ΔC_p value would be approximately 26 kJ mol^{-1} K^{-1}, if we take the heat capacity change observed for the 24-mer as basis, or about 11 kJ mol^{-1} K^{-1}, if we use the value for the 12-mer. Even the smaller value would be considered significant for a protein of molar mass 20000. The $\Delta H°$ values at T_m obtained by DSC and UV melting studies agree well, as can be seen in Table 4. This is not completely unexpected, as in both cases, analysis is based on the two-state model. However, as mentioned before, UV melting curve analysis was completely insensitive to the magnitude of ΔC_p at T_m, which therefore could only be derived with confidence from DSC measurements.

It is important to note that we observed small differences between the enthalpies in phosphate and cacodylate buffer (Table 4). This finding is consistent with results of our previous study on the kinetics of dodecamer duplex formation,[1] where we had observed a significant influence of the buffer on the on-rate constants and the activation energies of 12-mer duplex formation. It is also in agreement with the recent observations of Alemayehu et al.[59] who reported an influence of buffer species on the thermodynamics of short DNA duplex dissociation. Melting of 18−22 bp-containing duplexes in phosphate buffer was characterized by about 12.6 kJ (mol)$^{-1}$ higher stability relative to melting the same oligonucleotides in cacodylate buffer.

An important issue concerns the molecular interpretation of the temperature dependence of the observed enthalpies. The pragmatic interpretation assumes an intrinsic variation of $\Delta H°$ with temperature, as long as there is no indication of coupled reactions involving structural changes of the individual single strands after or concomitant with the disruption of the duplex. Therefore, it is essential for a proper assignment of the origin of the heat capacity changes to examine the heat capacity profiles of the single strands as well as their optical melting curves. The results of these measurements on the single strands are shown in Figures 3c and 4b. It is quite obvious that neither the heat capacity curves nor the UV melting profiles provide an indication of a single strand transition in the relevant temperature range. One can infer neither a flat peak in the heat capacity curve nor a faint sigmoidal variation in the UV melting curves. One observes solely a gradual increase of both heat capacity and absorption with increasing temperature. The origin of these gradual changes of both heat capacity and UV absorption remains undetermined. It could be due to changes in hydration, ion binding, uncooperative unstacking of bases, or the excitation of other energy absorbing modes or processes; however, on the basis of our present experiments, we cannot assign the single strand behavior to any particular physical event.

There has been evidence that with some oligonucleotide sequences, the large observed heat capacity change could be explained by the occurrence of significant structure in the single strands at low temperature. Mikulecky and Feig found for the formation of duplexes from 13-mers that the ΔC_p observed by ITC could be accounted for entirely by progressive melting of the single strands.[60] The single strand optical melting parameters allowed the accurate prediction of the heat capacity changes observed by ITC.

Thus, the nonexistence of single strand melting transitions is the key difference between our and their oligonucleotides. The much higher propensity to intrastrand stacking interactions of the 13-mers used by Mikulecky and Feig is likely the result of the large number of 8 G-C base pairs and their designed pairwise contiguity within that oligonucleotide as compared to only 4 G-C pairs in the 12-mers employed by us. Therefore, it may be due to the special design of their oligonucleotides that the heat capacity change associated with duplex formation can be fully assigned to single strand melting.

Comparison of Experimental and Predicted Binding Constants for Duplex Formation of 12-mers and 24-mers. The rebirth of interest in duplex formation of oligonucleotides is largely due to their usage as capturing agents in gene chip and functionalized nanoparticle systems for biomedical applications.[61−64] For these systems to function optimally, it is of utmost importance to couple specificity of binding with high affinity for the complementary strand. The highest specificity is associated with full complementarity of single strands; favorable binding is guaranteed by strongly negative standard Gibbs energy changes, $\Delta G°$.

The standard Gibbs energy changes that we observed for duplex formation of our 12-mers are in line with reports in other studies. For example, Lang and Schwarz[44] determined for the formation of 10-mer DNA duplexes at 20 °C standard Gibbs energy changes of −37.0 ± 0.9 kJ mol^{-1}, which translates into

TABLE 5: Comparison of Hybridization Constants for 12-mer (Ia + Ib) and 24-mer (IIIa + IIIb) Duplex Formation in 10 mM NaH_2PO_4 and 100 mM NaCl, pH 7, Buffer[a]

T (°C)	$K_{hyb}^{12\text{-mer}}$ (M^{-1})[b]	$K_{hyb}^{12\text{-mer}}$ (M^{-1})[c]	$K_{hyb}^{12\text{-mer}}$ (M^{-1})[d]	$K_{hyb}^{24\text{-mer}}$ (M^{-1})[b]	$K_{hyb}^{24\text{-mer}}$ (M^{-1})[e]	$K_{hyb}^{24\text{-mer}}$ (M^{-1})[f]
10	6.45×10^{11}	3.22×10^{10}	2.90×10^{11}	1.03×10^{26}	7.87×10^{19}	8.67×10^{24}
15	4.95×10^{10}	7.89×10^{9}	4.13×10^{10}	4.74×10^{23}	9.87×10^{18}	1.17×10^{23}
20	3.49×10^{9}	1.78×10^{9}	5.78×10^{9}	2.13×10^{21}	9.41×10^{17}	1.59×10^{21}
25	3.19×10^{8}	3.61×10^{8}	7.96×10^{8}	1.18×10^{19}	6.96×10^{16}	2.17×10^{19}
30	3.17×10^{7}	6.60×10^{7}	1.10×10^{8}	7.40×10^{16}	3.82×10^{15}	3.01×10^{17}
35	3.35×10^{6}	1.10×10^{7}	1.45×10^{7}	6.80×10^{14}	1.90×10^{14}	4.21×10^{15}
40	3.83×10^{5}	1.75×10^{6}	1.95×10^{6}	4.29×10^{12}	7.23×10^{12}	5.97×10^{13}
45				5.20×10^{10}	2.28×10^{11}	8.58×10^{11}
50				9.72×10^{8}	6.03×10^{9}	1.25×10^{10}
55				1.57×10^{7}	1.35×10^{8}	1.86×10^{8}

[a] The data were calculated with the algorithm cited in refs 71 and 72 or eq 12 using the ΔC_p values observed by ITC and DSC. The experimental hybridization constant of the 24-mer determined by ITC at 55 °C is 0.23×10^8 M^{-1}. [b] Calculated using the model from refs 71 and 72 and a $\Delta C_p = 0$ kJ mol^{-1} K^{-1}. [c] Calculated using $\Delta C_p = -4.36$ kJ mol^{-1} K^{-1} obtained from ITC experiments. [d] Calculated using $\Delta C_p = -2.32$ kJ mol^{-1} K^{-1} obtained from DSC experiments. [e] Calculated using $\Delta C_p = -9.7$ kJ mol^{-1} K^{-1} obtained from ITC experiments. [f] Calculated using $\Delta C_p = -3.95$ kJ mol^{-1} K^{-1} obtained from DSC experiments.

a binding constant of 8.8×10^6 M^{-1}. Similar values were reported by Schwarz et al.[45] in a previous study. ITC studies on the formation of 8-mer duplexes in 10 mM sodium cacodylate buffer, pH 7, by Kaur et al.[46] resulted in a binding constant at 10 °C of 8.58×10^6 M^{-1}. Binding constants of 1.1×10^8 M^{-1} were observed by ITC titrations for duplex formation of 13-mers of high GC content.[60] Marky et al.[65] reported a binding constant for 20 °C of 5.1×10^7 M^{-1} for duplex formation of an undecamer having 7 G-C pairs. Complementary decameric single strands having four noncontiguous purines were reported to hybridize at 25 °C with a binding constant of 5.7×10^4 M^{-1}.[66] A parameter set for an undecamer duplex having 7 G-C pairs was provided by Kankia and Marky.[67] The binding constant observed for hybridization in 10 mM Hepes buffer and 100 mM NaCl, pH 7.5, 20 °C, was 7.8×10^6 M^{-1}. UV melting studies by Sugimoto et al.[68] on self-complementary hexamers and octamers resulted in strongly sequence-dependent binding constants at 37 °C, varying from 923 M^{-1} for octamers containing two G-C pairs to 1.0×10^6 M^{-1} for hexamer helices consisting exclusively of G-C pairs.

Thus, in summary, the binding constants, which we determined by ITC titrations for the formation of the 12-mer duplexes, are of a similar order of magnitude as obtained for other duplexes having about the same number of base pairs. However, the exact values and their temperature dependence cannot be expected to be predictable on the basis of the sequence alone, as not only the sequence content, that is, the % G-C pairs, but also the order, or context, of the base pairs determines stability.[70]

In DNA chemistry, it is a straightforward procedure to increase the length of the oligonucleotides to adjust for maximal affinity. From doubling the number of base pairs, one would expect an approximately corresponding increase in the value of $|\Delta G°|$ and consequently in the equilibrium constant. However, there are significant differences in the numerical values of $\Delta G°$ and the equilibrium constants depending on which extrapolation procedure is employed for the calculation. As we performed besides the ITC measurements also UV and DSC melting studies, we could estimate and compare binding constants of the same oligonucleotides using constant or temperature-dependent enthalpies. Routinely, UV melting curves are analyzed on the basis of the two-state model under the assumption of temperature-independent enthalpies and entropies. For non-self-complementary strands forming a duplex, the equilibrium constant at the melting temperature is $K(T_m) = 4/C_T$. Thus, all duplexes of the same strand concentration exhibit the same binding constant at their T_m. Length differences and sequence individualities are reflected in the individual melting temperature. The equilibrium constant is transformed into a standard Gibbs energy change, $\Delta G°$, and used, in conjunction with the transition enthalpy, to calculate the transition entropy and the $\Delta G°$ values at different temperatures. This procedure is standard in all prediction routines, and we listed in columns 2 and 5 of Table 5 the values obtained for our 12-mers and 24-mers with the online program provided by Markham and Zuker.[71,72] For demonstration of the errors involved in neglect of the heat capacity change, we provide in Table 5 the binding constants and the corresponding standard Gibbs energy changes calculated using the constant heat capacity changes determined by DSC and ITC in Figure 6.

It is well-known that very high binding constants beyond approximately 10^9 M^{-1} are difficult to measure directly by ITC due to instrumental limitations. These constraints eliminate the possibility to directly determine hybridization constants for 24-mer duplex formation at low temperature. Therefore, we conducted titrations at elevated temperatures, where the binding equilibrium is shifted toward a higher degree of single strand formation. Figure 1c shows the thermal titration at 55 °C. The starting enthalpy at low saturation corresponds to the value of the 24-mer at this temperature and is about twice that of the 12-mer. The titration curve is well resolved and contains a sufficiently large number of points in the transition region for a proper evaluation of the equilibrium constant. The binding constant obtained from the analysis of the data at 55 °C is 2.3×10^7 M^{-1}. As the 24-mer consists of two identical 12-mers in tandem arrangement, there is principally the possibility that between two complementary 24-mer strands overlapping binding via 12 base pairs occurs. That type of association would result in binding constants similar to those for 12-mer duplex formation, but it would also yield hybridization enthalpies typical of the 12-mer duplex. This was, however, not observed. To probe the stoichiometry and the binding characteristics of the 24-mer for the complementary 12-mer, we titrated the 24-mer **IIIa** with the complementary 12-mer **Ib** with the result shown in Figure 1d. It can be seen that two 12-mers bind to the 24-mer, and both the enthalpies and the binding constants are similar to the values observed for complex formation between complementary 12-mers (Table 2).

Comparable binding constants for 24-mer duplexes from literature are scarce. In particular, there are no direct ITC measurements but only extrapolated data mainly from UV melting studies. Data for 10 °C from Vallone and Benight[69] on

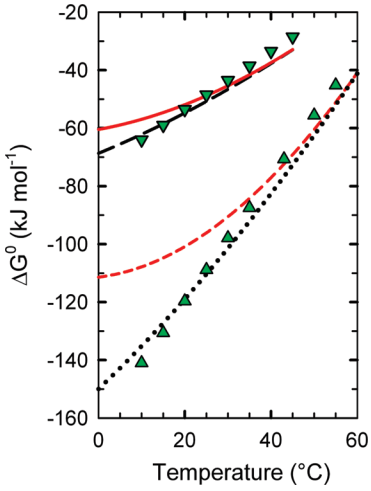

Figure 6. Stability curves of 12-mer (**Ia** + **Ib**) and 24-mer (**IIIa** + **IIIb**) duplexes. In the upper part, one finds the 12-mer stability curves. The green triangles represent the $\Delta G°$ calculated with the algorithm of refs 71 and 72 with a $\Delta C_p = 0$ kJ mol^{-1} K^{-1}; the black dashed line represents the $\Delta G°$ calculated using eq 8 with a $T_m = 322.77$ K (49.62 °C), $\Delta H° = -351$ kJ mol^{-1}, and $\Delta C_p = -2.32$ kJ mol^{-1} K^{-1} as obtained by DSC; the red solid curve represents the $\Delta G°$ calculated using eq 8 with identical T_m and $\Delta H°$ but $\Delta C_p = -4.4$ kJ mol^{-1} K^{-1} as determined by ITC. In the lower part of the figure are the 24-mer stability curves. The green triangles represent the $\Delta G°$ calculated with the algorithm of refs 71 and 72 calculated with a $\Delta C_p = 0$ kJ mol^{-1} K^{-1}; the black dotted curve represents the $\Delta G°$ calculated using eq 8 with $T_m = 338.25$ K (65.1 °C), $\Delta H° = -792$ kJ mol^{-1}, and $\Delta C_p = -3.95$ kJ mol^{-1} K^{-1} as obtained by DSC; the red dashed curve represents the $\Delta G°$ calculated using eq 8 with identical T_m and $\Delta H°$ but with $\Delta C_p = -9.7$ kJ mol^{-1} K^{-1} as determined by ITC.

40 base pair duplexes with GC content varying from 10 to 90% range from $\Delta G° = -158.6$ kJ (mol)$^{-1}$, which corresponds to an apparent binding constant of $K_B = 1.9 \times 10^{29}$ M^{-1} to $\Delta G° = -246$ kJ (mol)$^{-1}$ corresponding to $K_B = 2.5 \times 10^{45}$ M^{-1}. When the same oligonucleotides were studied by DSC, the standard Gibbs energy changes obtained deviated significantly from the parameters derived from the UV melting curves. Not only was the magnitude considerably higher but also the apparent correlation between the GC content and the $\Delta G°$ values at 10 °C was lost. In a DSC and UV melting study on six 22-mer duplexes having different end sequences, Riccelli et al.[70] reported $\Delta G°$ values at 20 °C ranging from -78.7 kJ (mol)$^{-1}$ to -193 kJ (mol)$^{-1}$ with the corresponding binding constants $K_B = 1.06 \times 10^{14}$ M^{-1} and $K_B = 2.5 \times 10^{34}$ M^{-1}. In an extensive DSC study on the influence of phosphate and cacodylate buffer on the thermodynamics of short DNA duplex melting, Alemayehu et al.[66] listed among others also $\Delta G°$ data for 25 °C. In phosphate buffer and in the presence of 1 M NaCl, the extrapolated values for 22-mers are spread between -99 kJ (mol)$^{-1}$ ($K_B = 2.2 \times 10^{17}$ M^{-1}) and -133 kJ (mol)$^{-1}$ ($K_B = 2.0 \times 10^{23}$ M^{-1}). The extrapolations to 25 °C from the melting temperatures were made on the assumption that $\Delta C_p = 0$, although several of the DSC curves shown in the supplementary data section apparently exhibit positive, nonzero ΔC_p values. Both the high NaCl concentration in the buffer and the neglect of ΔC_p in the extrapolation procedure tendentiously favor high $\Delta G°$ values. However, altogether, these extrapolated stabilities for 22-mer duplexes are of similar order of magnitude as the values obtained in the present study for the 24-mers.

To provide an illustration of the differences between stability predictions with and without consideration of the temperature dependence of the hybridization enthalpy, we show in Figure 6 stability curves of the 12-mers and 24-mers. They were calculated with eq 8 using the limiting ΔC_p values at low and high temperature determined by ITC and DSC. For comparison, the linear predictions resulting from the algorithm of Markham and Zuker are included.[71,72] It is clear that deviations are smallest in the case of small heat capacity changes and around room temperature. At low and high temperatures and in the presence of large ΔC_p values, the linear predictions are significantly off. We also realized a difference between the predicted value of the melting temperature (61.9 °C) of the 24-mer duplex and the experimental value of 65.1 °C. Thus, for a first estimate of Gibbs energy changes of short duplexes, the algorithm is a good choice; for more accurate thermodynamic parameters such as transition enthalpies and melting temperatures under special environmental conditions, a careful experiment is unavoidable.

Conclusions

The extensive ITC measurements and DSC and UV melting studies on two pairs of sequence-modified cDNA 12-mers and one pair of complementary 24-mer strands, constructed in tandem arrangement from two 12-mers of type **Ia** and **Ib**, respectively, permit a number of conclusions of general significance.

(1) For a first estimate of enthalpies and $\Delta G°$ values in the vicinity of 25 °C prediction schemes, such as that of Markham and Zuker used in the present study, are very valuable. (2) Estimates of thermodynamic parameters for temperatures away from ambient values can be significantly incorrect, because generally double helix formation is coupled to significant heat capacity changes. (3) At temperatures well below the melting temperature of the double helix, enthalpies and heat capacity changes can be determined best by ITC measurements. Measurements at T_m are preferably done by DSC. (4) Concentration-dependent T_m shift studies and optical melting curves are a valuable compliment for mechanistic analysis of helix formation but only of limited value for the determination of thermodynamic parameters. This deficiency is mainly due to the difficulty of determining heat capacity changes with any degree of certainty. (6) Binding constants of DNA duplexes having more than approximately 12 base pairs can be determined by ITC only at temperatures high enough to decrease binding constants to values in the detectable range ($\leq 10^9$ M^{-1}).

Acknowledgment. This work was supported by a research grant from Bundesministerium für Bildung und Forschung (BMBF) to H.-J.H. We thank Nhat Tran of Chembiotech (at CeNTech) for the synthesis of the oligonucleotides and Dr. H. Luftmann for the characterization by MALDI spectrometry. We also thank Dr. B. Beerman for helpful discussions and J. Guddorf for her excellent technical assistance.

References and Notes

(1) Carrillo-Nava, E.; Mejía-Radillo, Y.; Hinz, H.-J. Dodecamer DNA duplex formation is characterized by second-order kinetics, positive activation energies, and a dependence on sequence and Mg^{2+} ion concentration. *Biochemistry* **2008**, *47*, 13153–13157.

(2) Kallenbach, N. R.; Crothers, D. M.; Mortimer, R. G. Interpretation of kinetics of helix formation. *Biochem. Biophys. Res. Commun.* **1963**, *11*, 213–216.

(3) Crothers, D. M.; Kallenbach, N. R.; Zimm, B. H. Melting transtion of low-molecular-weight DNA—Theory and experiment. *J. Mol. Biol.* **1965**, *11*, 802–820.

(4) Pörschke, D.; Eigen, M. Co-operative non-enzymic base recognition. III Kinetics of the helix-coil transition of the oligoribouridylic oligoriboadenylic acid system and of oligoriboadenylic acid alone at acidic pH. *J. Mol. Biol.* **1971**, *62*, 361–381.

(5) Gray, D. M.; Ratliff, R. L.; Williams, D. L. Circular-dichroism of poly d(AAT):d(ATT) and poly r(AAU):r(AUU). Test of the first-neighbor hypothesis. *Biopolymers* **1973**, *12*, 1233–1245.

(6) Pörschke, D.; Uhlenbeck, O. C.; Martin, F. H. Thermodynamics and kinetics of the helix-coil transition of oligomers containing GC base pairs. *Biopolymers* **1973**, *12*, 1313–1335.

(7) Szabo, P.; Elder, R.; Uhlenbeck, O. C. Kinetics of in situ hybridization. *Nucleic Acids Res.* **1975**, *2*, 647–653.

(8) Hinz, H.-J.; Schmitz, O. J.; Ackermann, T. Calorimetric studies on melting of tRNA Phe (yeast). *Eur. J. Biochem.* **1969**, *72*, 79–86.

(9) Hinz, H.-J.; Schmitz, O. J.; Ackermann, T. Calorimetric investigation of the influence of polymer concentration on the transition enthalpy in the helix-coil transition of the double-stranded helical complex poly(A+U). *Biopolymers* **1969**, *7*, 611–613.

(10) Hinz, H. J.; Haar, W.; Ackermann, T. Experimental thermodynamics of the helix-random coil transition III. Determination of the transition enthalpies of the helical complexes poly(I+C) and poly I in solution. *Biopolymers* **1970**, *9*, 923–936.

(11) Rawitscher, M. A.; Ross, P. D.; Sturtevant, J. M. The heat of reaction between polyriboadenylic acid and polyuridylic acid. *J. Am. Chem. Soc.* **1963**, *85*, 1915–1918.

(12) Schena, M.; Shalon, D.; Davis, R. W.; Brown, P. O. Quantitative monitoring of gene expression patterns with a complementary DNA microarray. *Science* **1995**, *20*, 464–467.

(13) Mirkin, C. A.; Letsinger, R. L.; Mucic, R. C.; Storhoff, J. J. A DNA-based method for rationally assembling nanoparticles into macroscopic materials. *Nature* **1996**, *382*, 607–609.

(14) Loweth, C. J.; Caldwell, B. W.; Peng, X.; Alivisatos, A. P.; Schultz, P. G. DNA-based assembly of gold nanocrystals. *Angew. Chem., Int. Ed.* **1999**, *38*, 1808–1812.

(15) Storhoff, J. J.; Mirkin, C. A. Programmed materials synthesis with DNA. *Chem. Rev.* **1999**, *99*, 1849–1862.

(16) Taton, T. A.; Lu, G.; Mirkin, C. A. Two-color labeling of oligonucleotide arrays via size-selective scattering of nanoparticle probes. *J. Am. Chem. Soc.* **2001**, *123*, 5164–5165.

(17) Niemeyer, C. M.; Mirkin, C. A. *Nanobiotechnology. Concepts, Applications and Perspectives*; Wiley-VCH: Weinheim, Germany, 2004.

(18) Hazakira, P.; Ceyhan, B.; Niemeyer, C. M. Reversible switching of DNA-gold nanoparticle aggregation. *Angew. Chem., Int. Ed.* **2004**, *43*, 6469–6471.

(19) Park, S.-J.; Lazarides, A. A.; Storhoff, J. J.; Pesce, L.; Mirkin, C. A. The structural characterization of oligonucleotide-modified gold nanoparticle networks formed by DNA hybridization. *J. Phys. Chem. B* **2004**, *108*, 12375–12380.

(20) Dillenback, L. M.; Goodrich, G. P.; Keating, C. D. Temperature-programmed assembly of DNA:Au nanoparticle bioconjugates. *Nano Lett.* **2006**, *6*, 16–23.

(21) Hazarika, P.; Kukolka, F.; Niemeyer, C. M. Reversible binding of fluoroscent proteins at DNA-gold nanoparticles. *Angew. Chem., Int. Ed.* **2006**, *45*, 6827–6830.

(22) Seferos, D. S.; Prigodich, A. E.; Giljohann, D. A.; Patel, P. C.; Mirkin, C. A. Polyvalent DNA nanoparticle conjugates stabilize nucleic acids. *Nano Lett.* **2009**, *9*, 308–311.

(23) Breslauer, K. J.; Frank, R.; Blocker, H.; Marky, L. A. Predicting DNA duplex stability from the base sequence. *Proc. Natl. Acad. Sci. U.S.A.* **1986**, *83*, 3746–3750.

(24) SantaLucia, J., Jr. A unified view of polymer, dumbbell, and oligonucleotide DNA nearest-neighbor thermodynamics. *Proc. Natl. Acad. Sci. U.S.A.* **1998**, *95*, 1460–1465.

(25) SantaLucia, J., Jr.; Allawi, H. T.; Seneviratne, P. A. Improved nearest neighbour parameters for predicting DNA duplex stability. *Biochemistry* **1996**, *35*, 3555–3562.

(26) Gray, D. M. Derivation of nearest-neighbour parameters from data on nucleic acid oligomers. II. Thermodynamic parameters of DNA-RNA hybrids and DNA duplexes. *Biopolymers* **1997**, *42*, 795–810.

(27) Sugimoto, N.; Nakano, S.-I.; Misa, K.; Matsumura, A.; Nakamuta, H.; Ohmichi, T.; Yoneyama, M.; Sasaki, M. Thermodynamic parameters to predict stability of RNA/DNA hybrid duplexes. *Biochemistry* **1995**, *34*, 11211–11216.

(28) Xia, T.; SantaLucia, J., Jr.; Burkard, M. E.; Kierzek, R.; Schroeder, S. J.; Jiao, X.; Cox, C.; Turner, D. H. Thermodynamic parameters for an expanded nearest neighbor model for formation of RNA duplexes with Watson-Crick base pairs. *Biochemistry* **1998**, *37*, 14719–14730.

(29) Shiao, D. D. F.; Sturtevant, J. M. Heats of thermally induced helix-coil transitions of DNA in aqueous solution. *Biopolymers* **1973**, *12*, 1829–1836.

(30) Wu, P.; Nakano, S.; Sugimoto, N. Temperature dependence of thermodynamic properties for DNA/DNA and RNA/DNA duplex formation. *Eur. J. Biochem.* **2002**, *269*, 2821–2830.

(31) Filimonov, V. V. *The Thermodynamics of Conformation Transitions in Polynucleotides in Thermodynamic Data for Biochemistry and Biotechnology*; Hinz, H.-J., Ed.; Springer Verlag: Berlin, 1986; pp 377−401.

(32) Breslauer, K. J.; Sturtevant, J. M.; Tinoco, I., Jr. Calorimetric and spectroscopic investigation of the helix-to-coil transition of a ribo-oligonucleotide: rAU7. *J. Mol. Biol.* **1975**, *99*, 549–565.

(33) Filimonov, V. V.; Privalov, P. L. Thermodynamics of base interaction in (A)n and (A.U)n. *J. Mol. Biol.* **1978**, *122*, 465–470.

(34) Korolev, N.-L.; Vlasov, A. P.; Kuznetzov, I. A. Thermal denaturation of Na- and Li-DNA in salt-free solutions. *Biopolymers* **1994**, *34*, 1275–1290.

(35) Nordmeier, E. Effects of pressure on the helix-coil transition of calf thymus DNA. *J. Phys. Chem.* **1992**, *96*, 1494–1501.

(36) Ladbury, J. E.; Sturtevant, J. M.; Leontis, N. B. The thermodynamics of formation of a three-strand, DNA three-way junction complex. *Biochemistry* **1994**, *33*, 6828–6833.

(37) Freier, S. M.; Sugimoto, N.; Sinclair, A.; Alkema, D.; Neilson, T.; Kierzek, R.; Caruthers, M. H.; Turner, D. H. Stability of XGCGCp GCGCYp, and XGCGCYp helixes: An empirical estimate of the energetics of hydrogen bonds in nucleic acids. *Biochemistry* **1986**, *25*, 3214–3219.

(38) Lu, M.; Guo, Q.; Marky, L. A.; Seeman, N. C.; Kallenbach, N. R. Thermodynamics of DNA branching. *J. Mol. Biol.* **1992**, *223*, 781–789.

(39) Vesnaver, G.; Breslauer, K. J. The contribution of DNA single-stranded order to the thermodynamics of duplex formation. *Proc. Natl. Acad. Sci. U.S.A.* **1991**, *88*, 3569–3573.

(40) Mikulecky, P. J.; Feig, A. L. Heat capacity changes associated with nucleic acid folding. *Biopolymers* **2006**, *82*, 35–58.

(41) Salim, N. N.; Feig, A. L. Isothermal titration calorimetry of RNA. *Methods* **2009**, *47*, 198–205.

(42) Chalikian, T. V.; Beletskaya, I. V.; Chalikian, T. V. Stability of duplexes containing GG, CC, AA, and TT mismatches. *Biochemistry* **2006**, *45*, 10563–10571.

(43) Chalikian, T. V.; Völker, J.; Plum, G. E.; Breslauer, K. J. A more unified picture for the thermodynamics of nucleic acid duplex melting: A characterization by calorimetric and volumetric techniques. *Proc. Natl. Acad. Sci. U.S.A.* **1999**, *96*, 7853–7858.

(44) Lang, B. E.; Schwarz, F. P. Thermodynamic dependence of DNA/DNA and DNA/RNA hybridization reactions on temperature and ionic strength. *Biophys. Chem.* **2007**, *131*, 96–104.

(45) Schwarz, F. P.; Robinson, S.; Butler, J. Thermodynamic comparison of PNA/DNA and DNA/DNA hybridization reactions at ambient temperature. *Nucleic Acids Res.* **1999**, *27*, 4792–4800.

(46) Kaur, H.; Wengel, J.; Maiti, S. Thermodynamics of DNA-RNA heteroduplex formation: Effects of locked nucleic acid nucleotides incorporated into the DNA strand. *Biochemistry* **2008**, *47*, 1218–1227.

(47) Caruthers, M. H. Gene synthesis machines: DNA chemistry and its uses. *Science* **1985**, *230*, 281–285.

(48) Cantor, C. R.; Warshaw, M. M.; Shapiro, H. Oligonucleotide interactions. III. Circular dichroism studies of the conformation of deoxyoligonucleotides. *Biopolymers* **1970**, *9*, 1059–1077.

(49) Fasman, G. D., Ed. *Handbook of Biochemistry and Molecular Biology, Vol. 1: Nucleic Acids*, 3rd ed.; CRC Press: Cleveland, OH, 1975; p 589.

(50) Schwarz, F. P.; Reinisch, T.; Hinz, H.-J.; Surolia, A. Recommendations on measurement and analysis of results obtained on biological substances using isothermal titration calorimetry—(IUPAC technical report). *Pure Appl. Chem.* **2008**, *80*, 2025–2040.

(51) Wiseman, T.; Williston, S.; Brandts, J. F.; Lin, L.-N. Rapid measurement of Binding Constants and heats of Binding Using a New Titration Calorimeter. *Anal. Biochem.* **1989**, *179*, 131–137.

(52) Reinisch, T.; Hinz, H.-J. *Isothermal Titration Calorimetry in Encyclopedic Reference of Genomics and Proteomics in Molecular Medicine*; Ganten, D., Ruckpaul, K., Eds.; Springer: Berlin, Heidelberg, New York, 2006; pp 919−925.

(53) Rosgen, J.; Hinz, H.-J. Theory and practice of DSC measurements on proteins. In *Handbook of Thermal Analysis and Calorimetry*; Kemp, R. B., Ed.; Elsevier Science: Amsterdam, 1999; Vol. 4, pp 63−108.

(54) Durchschlag, H. Specific volumes of biological macromolecules and some other molecules of biological interest. In *Thermodynamic Data for Biochemistry and Biotechnology*; Hinz, H.-J., Ed.; Springer Verlag: Berlin, 1986; pp 45−128.

(55) Ababou, A.; Ladbury, J. E. Survey of the year 2005: Literature on applications of isothermal titration calorimetry. *J. Mol. Recognit.* **2007**, *20*, 4–14.

(56) Ababou, A.; Ladbury, J. E. Survey of the year 2006: Literature on applications of isothermal titration calorimetry. *J. Mol. Recognit.* **2008**, *19*, 79–89.

(57) Holbrook, J. A.; Capp, M. W.; Saecker, R. M.; Record, T. M., Jr. Enthalpy and heat capacity changes for formation of an oligomeric DNA duplex: Interpretation in terms of coupled processes of formation and association of single stranded helices. *Biochemistry* **1999**, *38*, 8409–8422.

(58) Schöppe, A.; Hinz, H.-J.; Rosemeyer, H.; Seela, F. Xylose-DNA: Comparison of the thermodynamic stability of oligo(2′-deoxyxylonucleotide) and oligo(2′-deoxyribonucleotide) duplexes. *Eur. J. Biochem.* **1996**, *239*, 33–41.

(59) Alemayehu, S.; Fish, D. J.; Brewood, G. P.; Horne, M. T.; Manyanga, F.; Dickman, R.; Yates, I.; Benight, A. S. Influence of buffer species on the thermodynamics of short DNA duplex melting: Sodium phosphate versus sodium cacodylate. *J. Phys. Chem. B* **2009**, *113*, 2578–2586.

(60) Mikulecky, P. J.; Feig, A. L. Heat capacity changes associated with DNA duplex formation: Salt- and sequence-dependent effects. *Biochemistry* **2006**, *45*, 604–616.

(61) Ma, X.; Yin, H.; Chen, K. Differential gene expression profiles in coronary heart disease patients of blood stasis syndrome in traditional Chinese medicine and clinical role of target gene. *Chin. J. Integr. Med.* **2009**, *15*, 101–106.

(62) Hsiao, C. R.; Huang, L.; Bouchara, J.-P.; Barton, R.; Li, H. C.; Chang, T. C. Identification of medically important molds by an oligonucleotide array. *J. Clin. Microbiol.* **2005**, *43*, 3760–3768.

(63) Lee, J.-S.; Mirkin, C. A. Chip-based scanometric detection of mercuric ion using DNA-functionalized gold nanoparticles. *Anal. Chem.* **2008**, *80*, 6805–6808.

(64) Witten, K. G.; Bretschneider, J. C.; Eckert, T.; Richtering, W.; Simon, U. Assembly of DNA-functionalized gold nanoparticles studied by UV/Vis-spectroscopy and dynamic light scattering. *Phys. Chem. Chem. Phys.* **2008**, *10*, 1870–1875.

(65) Marky, L. A.; Rentzeperis, D.; Luneva, N. P.; Cosman, M.; Geacintov, N. E.; Kipke, D. W. Differential hydration thermodynamics of stereoisomeric DNA-benzo[α] pyrene adducts derived from diol epoxide enantiomers with different tumorigenic potentials. *J. Am. Chem. Soc.* **1996**, *118*, 3804–3810.

(66) Ratilainen, T.; Holmen, A.; Tuite, E.; Haaima, G.; Christensen, L.; Nielsen, P. E.; Norden, B. Hybridization of peptide nucleic acid. *Biochemistry* **1998**, *37*, 12331–12342.

(67) Kankia, B. I.; Marky, L. A. DNA, RNA, and DNA/RNA oligomer duplexes: A comparative study of their stability, heat, hydration, and Mg^{2+} binding properties. *J. Phys. Chem. B* **1999**, *103*, 8759–8767.

(68) Sugimoto, N.; Honda, K.; Sasaki, M. Application of the thermodynamic parameters of DNA stability prediction to double-helix formation of deoxyribooligonucleotides. *Nucleosides, Nucleotides Nucleic Acids* **1994**, *13*, 1311–1317.

(69) Vallone, P. M.; Benight, A. S. Thermodynamic, spectroscopic, and equilibrium binding studies of DNA sequence context effects in six 22-base pair deoxyoligonucleotides. *Biochemistry* **2000**, *38*, 11197–11208.

(70) Riccelli, P. V.; Vallone, P. M.; Kashin, I.; Faldasz, B. D.; Lane, M. L.; Benight, A. S. Thermodynamic, spectroscopic, and equilibrium binding studies of DNA sequence context effects in six 22-base pair deoxyoligonucleotides. *Biochemistry* **1999**, *38*, 11197–11208.

(71) Markham, N. R.; Zuker, M. DINAMelt web server for nucleic acid melting prediction. *Nucleic Acids Res.* **2005**, *33*, W577–W581.

(72) Markham, N. R.; Zuker, M. UNAFold: Software for nucleic acid folding and hybriziation. In *Bioinformatics, Vol. II. Structure, Functions and Applications*; Keith, J. M., Ed.; Humana Press: Totowa, NJ, 2008; Methods in Molecular Biology, Chapter 1, pp 3−31.

JP100412A